Dynamic Decision Model for Tunnel Cross-Passage Layout Based on Multi-Source Sensor Data Fusion

Xuejun Di[1]*, Musha Ruzi[2], Angang Liu[3]
China First Highway Engineering Co., Ltd., Beijing 100010, China[1]
Safety and Quality Department, Xinjiang Uygur Autonomous Region Transportation Construction Affairs Center, Urumqi 830000, Xinjiang, China[2]
Engineering and Technology Department, Xinjiang Uygur Autonomous Region Transportation Construction Affairs Center, Urumqi 830000, Xinjiang, China[3]

***Abstract*—The layout of tunnel cross-passages is a critical aspect of tunnel construction and operational safety. Traditional methods, primarily based on static design, struggle to adapt to complex and variable geological and construction environments. This study proposes a dynamic decision model for cross-passage layout based on multi-source sensor data fusion to enhance the scientific rigor and adaptability of cross-passage design. A three-dimensional data fusion mechanism integrating "temporal-spatial-statistical" dimensions was developed. Bayesian network quantifies uncertainty, Kalman filter processes time series data, and PCA extracts spatial features. Reinforcement learning and non-dominated sorting genetic algorithm II (NSGA-II) are used to achieve multi-objective optimization of safety coverage and construction efficiency. The proposed model significantly outperforms the traditional methods in many indicators, and is verified by 100 Monte Carlo simulations and actual tunnel experiments. The dynamic scheme increased the safety coverage rate from 72.4% to 91.7%, shortened the average evacuation distance by 38.7% (from 248 meters to 152 meters), saved resources by 14.2% (about 9.8 million yuan), and shortened the construction period by 3-6 days. The comprehensive utility value is 0.91, which is 19% higher than the traditional static method, and the robustness is enhanced. The model realizes the safe, economical, and efficient real-time optimization of the layout of the transverse channel. It provides a technical path and data support that can be promoted for intelligent tunnel construction under complex geological conditions.**

***Keywords*—Multi-source sensor data fusion; dynamic cross-passage deployment decision-making for tunnels; Kalman filter; reinforcement learning; non-dominated sorting genetic algorithm II**

I. Introduction

With the continuous advancement of infrastructure development in China, tunnel engineering has assumed an increasingly vital role in transportation, water conservancy, power, and other sectors [1-2]. Particularly under the "Transportation Powerhouse" strategy, projects involving long tunnels, deep-buried tunnels, and tunnels in complex geological conditions are proliferating. The tunnel length, burial depth and geological complexity of the national key projects such as the Dianzhong Water Diversion Project, the Sichuan-Tibet Railroad and the Shenzhen-Zhongshan Channel are all ranked first in the world [3]. As an important part of the tunnel structure system, the cross passage performs various functions during the construction process, including ventilation, transportation, evacuation, and drainage. During operation, it also undertakes important responsibilities such as disaster prevention and rescue, equipment maintenance and partition management [4]. In order to ensure safety, improve operational efficiency and reduce engineering risks, the cross passage must be arranged scientifically and reasonably [5].

However, traditional cross-passage layout methods primarily rely on static geological surveys and empirical judgments during the design phase, employing fixed intervals or simple rules for placement. This approach lacks responsiveness to dynamic factors such as geological changes during construction, construction disturbances, and resource scheduling [6]. In complex geological conditions—such as karst formations, faults, gas-bearing zones, and rockburst-prone sections—static placement often results in suboptimal cross-passage locations, redundant or insufficient quantities, thereby compromising construction safety and efficiency, and potentially triggering engineering accidents [7-8].

In recent years, rapid advancements in IoT, artificial intelligence, and sensing technologies have generated increasingly rich multi-source heterogeneous data during tunnel construction. This includes georadar (GPR), seismic wave detection (TSP), advance drilling, construction progress monitoring, personnel positioning, environmental monitoring, and material consumption data [9]. These data provide an unprecedented information foundation for dynamically optimizing cross-passage placement. Effectively integrating these multi-source sensor data to construct a dynamic deployment decision model with real-time response capability has become a critical scientific issue for the intelligent development of tunnel engineering. Key research areas in constructing dynamic deployment decision models for tunnel cross passages include multi-source data fusion mechanism design [10], dynamic decision model construction [11], simulation verification, and engineering applications [12]. Currently, universities and research institutions worldwide have made significant progress in tunnel intelligence. Tang et al. [13] achieved advance warning for poor geological sections in a mountain tunnel project by integrating ground-penetrating radar with TSP data. Andrade-Lucio et al. [14] established a full-lifecycle health monitoring system for tunnels by deploying thousands of sensors. Overseas research has primarily focused on structural health monitoring and disaster early warning, with limited studies on dynamic deployment for ancillary structures

*Corresponding author.

like cross passages, and no systematic decision models have yet been developed. In China, geological advance prediction, construction risk early warning, and BIM+GIS integrated management are all hot topics [15]. Support vector machine (SVM) data and construction data can be used to predict the risk of tunnel collapse [16]. In addition, Luo et al. [17] proposed a cross-passage spacing optimization method based on a genetic algorithm. The current research has the following shortcomings: most studies only focus on the optimization of the design stage, while ignoring the dynamic evolution in the construction process [18]; a single algorithm is mainly used for shallow data fusion, which cannot completely solve the spatiotemporal heterogeneity and uncertainty [19]; some studies only focus on algorithm development without considering actual engineering data, which leads to insufficient transferability and practicality [20].

Addressing these issues and challenges, this study proposes a dynamic cross-passage deployment decision model based on multi-source sensor data fusion. The main contributions are as follows: 1) A three-dimensional fusion mechanism of "spatiotemporal statistics" is introduced, Kalman filtering is used to process time-series data, PCA is used to extract spatial features, and Bayesian network is used to quantify uncertainty, so as to realize the efficient fusion of geological, construction and resource data; 2) A reinforcement learning-oriented cross-passage layout optimization model driven by the dual objectives of safety coverage and construction efficiency is constructed to realize real-time decision-making update in the construction process; 3) A high-fidelity simulation environment is established based on tunnel engineering data, and the model performance is evaluated from multiple dimensions such as safety, economy and adaptability.

The structure of this study is as follows: Section II introduces fundamental methods and typical applications of multi-source sensor data fusion, providing a theoretical foundation for decision model construction. Section III analyzes traditional methods for deploying cross-tunnel sensors and the advantages of dynamic deployment, clarifying the research questions and objectives. Section IV proposes a dynamic deployment decision model based on multi-source sensor data fusion, including the overall framework, data fusion mechanism, and a hybrid optimization method combining reinforcement learning with NSGA-II. Section V evaluates the model's performance through simulation experiments and field validation, focusing on comparative analysis of safety, efficiency, and cost-effectiveness. Finally, Section VI summarizes key findings, identifies research limitations, and proposes future research directions.

II. Multi-Source Sensor Data Fusion Technology

A. Data Fusion Methods and Algorithms

Multi-source Sensor Data Fusion (MSDF) [21] refers to the comprehensive processing of data from different sensors, different times, different spaces, or different modalities to obtain information that is more accurate, reliable, and comprehensive than that from a single data source. Its core objectives are to eliminate redundancy, suppress noise, fill in missing data, and enhance the robustness and real-time capability of decision-making [22]. Fig. 1 illustrates the definition of multi-source sensor data fusion methods.

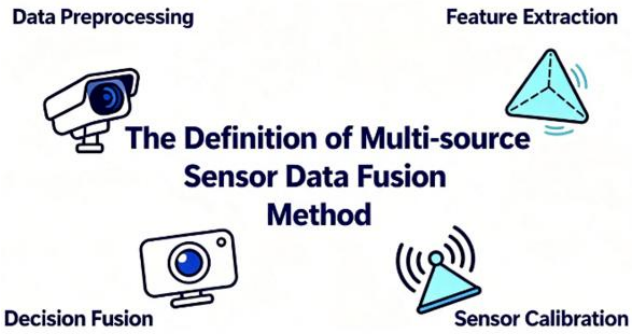

Fig. 1. Definition of multi-source sensor data fusion methods.

Based on the level of data abstraction, fusion methods are typically categorized into three tiers: data-level fusion, feature set fusion, and decision-level fusion [23]. Table I illustrates the hierarchical classification of multi-source sensor data fusion methods and algorithm categories. Table I indicates that data-level fusion methods include weighted averaging and Kalman filtering algorithms; feature-level fusion methods encompass PCA, ICA, and wavelet transforms; while decision-level fusion methods involve Bayesian inference, D-S evidence theory, and voting methods.

TABLE I. Hierarchy and Algorithms of Multi-Source Sensing Data Fusion Methods

Level	Name	Description	Common Methods
L1	Data-level fusion	Raw data was directly merged most information was retained	Weighted average Kalman filter
L2	Feature-level fusion	Features extracted, then fused, dimensionality reduced	PCA ICA Wavelet transform
L3	Decision-level fusion	Each source makes an independent decision and then fuses the results	Bayesian inference D-S evidence theory Voting method

The Kalman filter (KF) is suitable for linear dynamic systems in Gaussian noise environments and can recursively estimate the system state [24]. Fig. 2 shows the prediction and update process of the KF algorithm, which mainly consists of the update step and the prediction step.

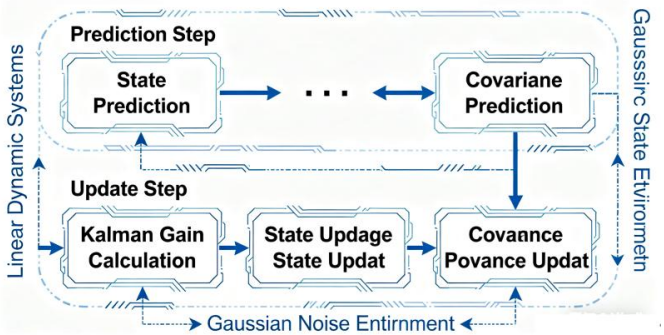

Fig. 2. KF algorithm workflow diagram.

Principal Component Analysis (PCA) is employed for dimensionality reduction and feature extraction in high-dimensional data, eliminating redundant dimensions while retaining the directions of maximum variance [25]. The PCA method calculates the covariance matrix as follows:

$$\boldsymbol{C} = \frac{1}{n-1}\boldsymbol{X}^T\boldsymbol{X} \tag{1}$$

where, $\boldsymbol{C}$ denotes the covariance matrix, n represents the number of data samples, and $\boldsymbol{X}$ indicates the sample data. The feature decomposition calculation is analyzed as follows:

$$\boldsymbol{C}v_i = \lambda_i v_i, \lambda_1 \geq \lambda_2 \geq \mathrm{L} \geq \lambda_d \tag{2}$$

Here, v_i denotes the i-th eigenvector, and λ_i denotes the i-th eigenvalue. Select the first k principal components such that their cumulative contribution rate $\geq 95\%$:

$$CPV_k = \frac{\sum_{i=1}^{k}\lambda_i}{\sum_{i=1}^{d}\lambda_i} \tag{3}$$

Here, CPV_k denotes the cumulative contribution rate of the k-th eigenvector. Based on the above PCA principles, the PCA dimension reduction process is summarized in Fig. 3.

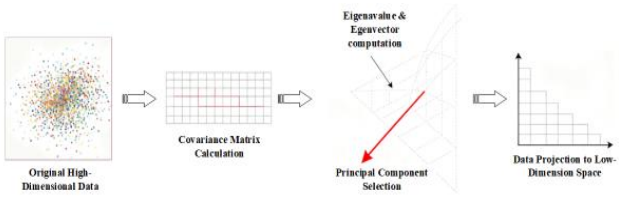

Fig. 3. Schematic diagram of PCA dimension reduction.

Bayesian estimation and decision fusion methods are suitable for scenarios with high uncertainty and abundant prior knowledge [26]. The posterior distribution is obtained through the likelihood function and prior distribution [see Eq. (4)]:

$$P(\theta|z) = \frac{P(z|\theta)P(\theta)}{P(z)} \tag{4}$$

where, $P(\theta|z)$ denotes the posterior distribution probability, $P(z|\theta)$ represents the likelihood function, $P(\theta)$ indicates the prior probability, $P(z)$ signifies the evidence, θ denotes the Bayesian parameter, and z refers to the observed data.

B. Applications of Fusion Techniques Across Domains

Intelligent transportation systems, environmental monitoring, industrial equipment fault diagnosis, and healthcare are all fields in which multi-source sensor data fusion technology is widely used [27]. Fig. 4 shows the application analysis of fusion technology in various fields.

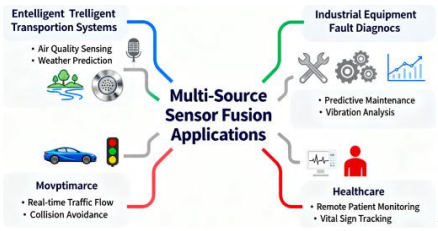

Fig. 4. Analysis of fusion technology applications across different fields.

In intelligent transportation, multi-source data fusion technology is used for traffic flow monitoring, accident detection, and vehicle navigation. Tomaszewski et al. [28] point out that traffic conditions can be monitored by integrating camera, radar, and GPS data, congestion can be predicted, and the best route suggestions can be provided for drivers.

In environmental monitoring, multi-source sensor data fusion technology is applied to air quality monitoring, water quality monitoring, and natural disaster early warning. Zhao et al. [29] demonstrate that by integrating data from ground monitoring stations, satellite remote sensing, and drones, real-time monitoring and dispersion prediction of atmospheric pollutants can be achieved. Applications of data fusion in environmental monitoring are shown in Table II.

TABLE II. APPLICATIONS OF DATA FUSION IN ENVIRONMENTAL MONITORING

Data Source	Fusion Method	Application Scenario	Advantage
Ground monitoring station	Kalman filter	Air quality monitoring	High accuracy real-time
Satellite remote sensing	PCA	Water quality monitoring	Dimensionality reduction, wide coverage
Drone	Bayesian estimation	Natural disaster warning	Uncertainty handling flexibility

By integrating data from machine vision, temperature, and pressure sensors, the running status of production line equipment can be monitored in real-time, potential faults can be predicted, and production processes can be optimized [30].

In the healthcare industry, data fusion technology is used for disease diagnosis, patient monitoring, and rehabilitation treatment [31]. The technology can monitor the health status of patients in real time and provide early warning by integrating physiological signals such as blood pressure, body temperature, and electrocardiogram (ECG).

III. DYNAMIC LAYOUT TECHNOLOGY FOR TUNNEL CROSS-PASSAGES

In tunnel engineering, the layout technology for cross-passages is undergoing a transformation from traditional to dynamic approaches. Although the traditional method meets the basic functional requirements of the tunnel, its limitations are becoming more and more obvious in complex geological conditions and a construction environment. On the other hand, the dynamic design technology shows its unique advantages with its high efficiency and flexibility.

A. Traditional Design Methods and Limitations

According to the Specifications for Design of Highway Tunnels (JTG D70-2022), the traditional tunnel cross passage layout mainly uses the empirical spacing method. This method is mainly based on the tunnel length, surrounding rock type, traffic level and other factors for one-time design. The layout remains largely unchanged during construction and rarely undergoes modification during the operational phase [32]. Fig. 5 illustrates the flowchart of the traditional layout method. However, this approach has significant limitations.

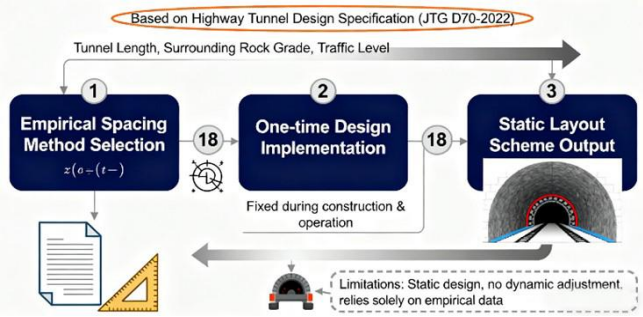

Fig. 5. Flowchart of traditional deployment method.

The static nature of traditional deployment methods makes it difficult to deal with sudden geological changes and construction disturbances. These techniques focus primarily on the spacing required by the specification, and ignore resource optimization and security redundancy. Over-deployment may increase engineering costs. The limitations of traditional layout methods can be further studied by combining the equations and parameter provisions related to the design specification of highway immersed tunnel.

B. Advantages of Dynamic Deployment Technology

Dynamic deployment technology overcomes the limitations of traditional methods and continuously integrates multi-source sensor data to update the position and number of cross-channels in real time [33]. Fig. 6 shows the dynamic deployment technology and its advantages:

Fig. 6. Dynamic layout technology.

1) Enhancing safety and emergency response capabilities: Dynamic layout can adjust the position of the cross passage in time according to the changes of geological conditions, so that personnel can be quickly evacuated in case of disaster. For example, the comprehensive advanced forecast system can accurately understand the geological conditions in front of the tunnel, so as to plan the position of the cross passage in advance, so as to reduce casualties and equipment losses.

2) Optimizing resource allocation and reducing costs: Compared with traditional technology, dynamic site selection reduces the construction of unnecessary transverse passages, thereby reducing the project cost. Under the premise of ensuring safety standards, dynamic route selection can greatly reduce the project cost in some auxiliary tunnels of the Sichuan-Tibet Railroad.

3) Enhancing construction efficiency: Through dynamic deployment, the construction of the transverse passage can be arranged reasonably according to the progress and resource consumption, so as to reduce the construction interference and improve the overall efficiency.

C. Analysis of Dynamic Cross-Passage Layout Decision-Making for Tunnels

The dynamic layout decision for tunnel cross-passages constitutes a complex multi-objective optimization problem [34], involving multiple variables and constraints. Fig. 7 illustrates the analysis of this decision-making problem.

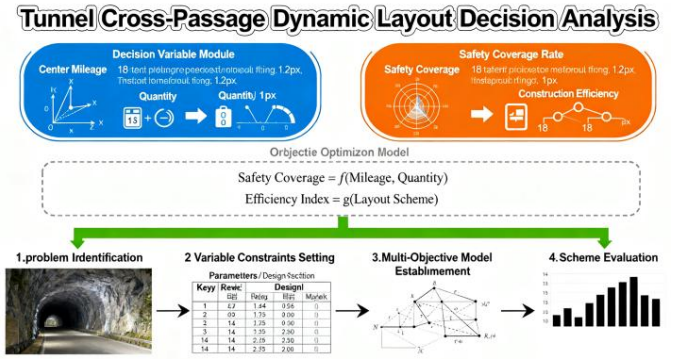

Fig. 7. Analysis of dynamic cross-passage layout decision problem in tunnels.

Decision variables include the center mileage and quantity of cross passages. The objective function typically establishes a multi-objective optimization model for cross-passage layout with dual targets: safety coverage rate and construction efficiency. The safety coverage rate is calculated as follows [see Eq. (5)]:

$$S_{\text{cov}-rate} = \frac{N_{\text{cov}-rate}}{N_{rate}} \times 100\% \tag{5}$$

where, $S_{\text{cov}-rate}$ denotes safety coverage rate, $N_{\text{cov}-rate}$ represents the proportion of personnel covered, and N_{rate} denotes the total personnel proportion.

Construction efficiency can be measured by the average evacuation time, Eq. (6):

$$T_{mean} = \frac{D_{esc}}{v_{esc}} \tag{6}$$

where, T_{mean} denotes average evacuation time, D_{esc} denotes total evacuation distance, and v_{esc} denotes evacuation speed.

Constraints primarily include geological safety, spacing limitations, construction interference, and resource caps. Geological safety constraints prohibit eliminating cross passages in areas with rock mass grades ≥ IV. Spacing constraints require cross passages to meet standard-specified distances. Construction interference constraints mandate reasonable scheduling of construction phases to avoid mutual disruption. Resource cap constraints reflect limited monthly excavation capacity.

IV. Construction of a Dynamic Cross-Passage Layout Decision Model

With the continuous advancement of tunnel construction technology, efficiently and safely laying out tunnel cross-passages has become a critical issue. In order to realize the real-time monitoring and dynamic optimization of tunnel construction process, this section introduces a dynamic cross-passage layout decision model based on multi-sensor data fusion.

A. Overall Framework

The model's overall framework, shown in Fig. 8, comprises four main layers: data acquisition, data fusion, decision-making, and execution. Let the data acquisition layer collect raw data from multiple sensors. These sensors include geological radar, seismic wave detection, advanced drilling, construction progress monitoring, personnel positioning and environmental monitoring. By processing these data with data fusion layer, the comprehensive evaluation of tunnel construction environment can be obtained. Based on the fused data, the decision-making layer uses reinforcement learning and multi-objective optimization algorithms to determine the optimal cross passage layout scheme. Finally, the execution layer uses the decision results for the construction and adjustment of the cross passage.

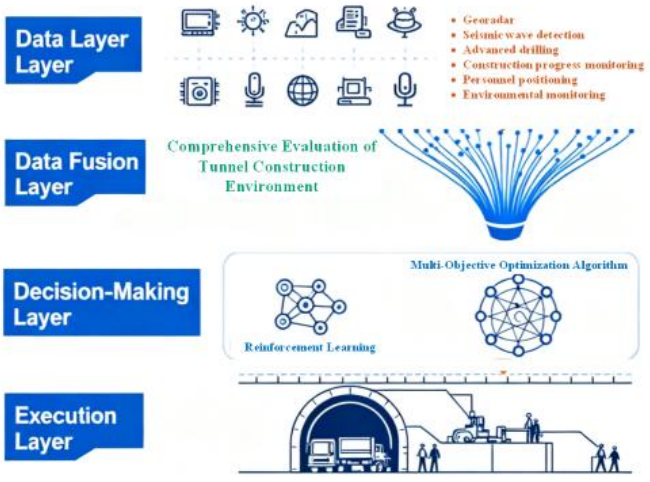

Fig. 8. Framework of the dynamic tunnel cross-passage layout decision model based on multi-source sensor data fusion.

B. Selection of Data Fusion Methods

At the data fusion layer, we employ multiple data fusion methods to handle different types of sensor data. This study uses Kalman filter to collect time series data, such as construction progress and resource consumption. Kalman filtering is a recursive estimation algorithm capable of effectively processing noisy data in dynamic systems. Its core equations are as follows [see Eq. (7) to Eq. (11)]:

$$\hat{x}_{k|k-1} = F_k \hat{x}_{k-1|k-1} + B_k u_k \tag{7}$$

$$P_{k|k-1} = F_k P_{k-1|k-1} F_k^T + Q_k \tag{8}$$

$$K_k = P_{k|k-1} H_k^T \left(H_k P_{k|k-1} H_k^T + R_k \right)^{-1} \tag{9}$$

$$\hat{x}_{k|k} = \hat{x}_{k|k-1} + K_k \left(z_k - H_k \hat{x}_{k|k-1} \right) \tag{10}$$

$$P_{k|k} = \left(1 - K_k H_k \right) P_{k|k-1} \tag{11}$$

Here, $\hat{x}$ denotes state estimation, P represents the estimation error covariance, F denotes the state transition model, B denotes the control input model, u denotes the control input, Q denotes the process noise covariance, z denotes the measurement value, H denotes the observation model, R denotes the measurement noise covariance, and K denotes the Kalman gain.

For spatial data such as ground-penetrating radar images, this study employs principal component analysis (PCA) for dimensionality reduction. PCA extracts key features from the data, reducing dimensionality while preserving critical information. The mathematical expressions for PCA are given in Eq. (1) to Eq. (3).

According to the above introduction and description, Table III summarizes the advantages and disadvantages of various data fusion methods.

TABLE III. Comparison of Different Data Fusion Methods

Method	Applicable Data Type	Advantage	Limitation
Kalman filter	Time series data	Handles noise in dynamic systems	Assumes linearity and Gaussian distribution
Principal component analysis	Spatial data	Extracts main features dimensionality reduction	Requires large data for training

C. Decision Model Design

The design of the decision model constitutes the core component of the entire system. We adopted a hybrid approach combining Reinforcement Learning (RL) [35] and the Non-Dominated Selection Genetic Algorithm II (NSGA-II) [36] to achieve multi-objective optimization between safety and cost. NSGA-II is used to find the Pareto optimal solution in multi-objective optimization; reinforcement learning is used to learn the most effective method through interaction with the

environment. Fig. 9 shows the teaching process of the hybrid reinforcement learning and NSGA-II model.

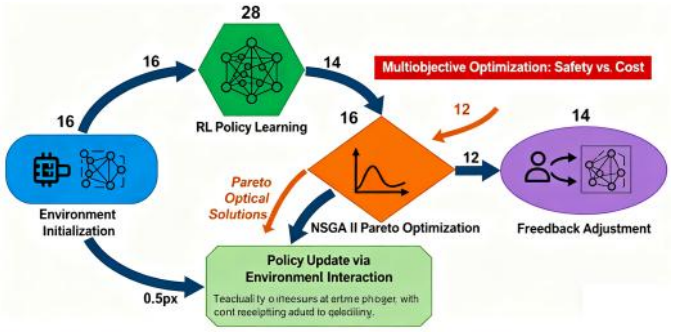

Fig. 9. Training process of the reinforcement learning and NSGA-II hybrid model.

In reinforcement learning, we defined the state space, action space, and reward function. The state space includes information such as geological conditions, construction progress, and resource consumption; the action space includes operations such as adding new cross passages, retaining existing cross passages, and canceling cross passages; the reward function comprehensively considers safety and cost factors [see Eq. (12)]:

$$R(s,a) = w_1 \Delta S + w_2 \Delta E - w_3 C_{cost} \tag{12}$$

where, w_1, w_2, and w_3 are weight coefficients, ΔS represents safety gains, ΔE represents efficiency gains, and C_{cost} represents cost penalties.

D. Model Validation and Optimization

To validate the model's effectiveness and robustness, this section conducts Monte Carlo simulations and field experiments. Monte Carlo simulations evaluate the model's performance under varying noise conditions, while field experiments validate its application in actual tunnel construction [37].

Fig. 10 illustrates the model performance under varying noise conditions, representing the Monte Carlo simulation results. To test the robustness of the model, Table IV shows the Monte Carlo simulation with different levels of Gaussian noise added to the sensor data. Results indicate that even at a 15% noise level, the model's hypervolume (HV) metric decreased by only 4%, demonstrating excellent robustness.

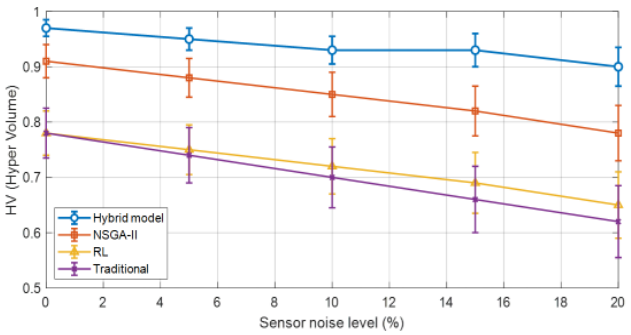

Fig. 10. Monte Carlo simulation results.

TABLE IV. COMPARISON OF MODEL VALIDATION RESULTS

Method	HV Index	Running Time/s	Adoption Rate
Traditional method	0.78	182	-
NSGA-II only	0.91	12	-
Reinforcement learning	0.78	0.3	-
Hybrid model	0.97	2.1	83%

E. Method Steps

Based on the aforementioned framework and methodology, the workflow for the tunnel cross-passage dynamic deployment decision-making model is illustrated in Fig. 11. The specific steps are as follows:

Step 1: Data Acquisition. Real-time collection of multi-source sensor data including ground-penetrating radar, seismic wave detection, and construction progress monitoring.

Step 2: Data Preprocessing. Cleaning, normalization, and time alignment of acquired data.

Step 3: Data Fusion. Integrate data using Kalman filtering and principal component analysis to form a comprehensive assessment of the tunnel construction environment.

Step 4: Decision Generation. Generate optimal cross-passage layout plans through a hybrid model of reinforcement learning and NSGA-II.

Step 5: Plan Execution. Guide the construction and adjustment of the cross passage, and apply the decision-making results to the actual construction.

Step 6: Feedback Optimization. Update the model parameters based on the actual construction results to better handle decision-making.

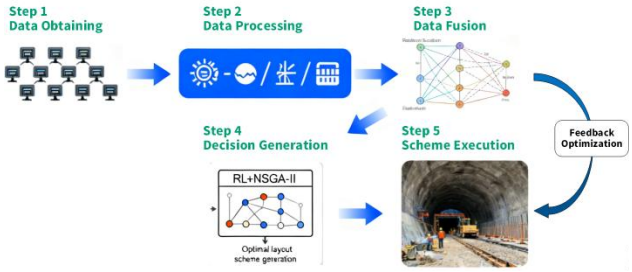

Fig. 11. Methodological flowchart for dynamic decision-making model of tunnel cross-passage layout.

V. EXPERIMENTAL VALIDATION

A. Experimental Design

For the experimental subject and scenario, this study selected a mountain tunnel project as the simulation object. The tunnel spans 4.8 kilometers, with surrounding rock classifications distributed across Grade II, III, IV, and V. Simulated construction scenarios encompass varying geological conditions and construction progress.

For data acquisition and processing, simulated sensors generate Ground Penetrating Radar (GPR), Transverse Seismic Profile (TSP), and construction progress monitoring data.

Preprocessing includes missing value imputation, normalization, time alignment, and outlier removal.

Data processing and model training were performed using MATLAB 2021a. A Monte Carlo method was employed to conduct 100 simulations, validating the model's robustness and effectiveness. Parameter settings for the reinforcement learning and NSGA-II hybrid model are presented in Table V.

TABLE V. PARAMETER SETTINGS FOR THE REINFORCEMENT LEARNING AND NSGA-II HYBRID MODEL

Parameter	Description	Value
Learning rate	Controls learning step size	0.01
Discount factor	Future reward discount rate	0.95
Weight coefficient	Weights for safety, efficiency, and cost	w1=0.6 w2=0.3 w3=0.1

B. Result Analysis

To evaluate the proposed method for constructing a dynamic cross-passage deployment decision model based on multi-source sensor data fusion, this section conducts simulation analysis across four dimensions: data generation and preprocessing, algorithm comparison, and deployment effectiveness assessment.

1) Data generation and preprocessing: To validate the effectiveness of the proposed data preprocessing method, analyses were conducted on rock mass classification, construction progress, resource consumption, and normalization. The specific results are as follows:

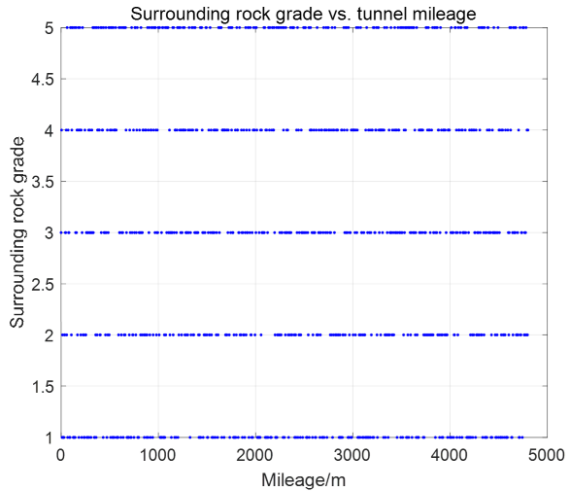

Fig. 12. Rock mass grade vs. Tunnel mileage.

Fig. 12 shows the distribution of rock mass grades (1~5) of about 5000 measuring points along the line, and the blue scatter points represent these grades. Poor rock mass sections (IV-V grade) appear continuously near 1.2 km, 3.1 km and 4.1 km, and the remaining sections are mainly II-III grade. This spatial differentiation shows three high-risk areas, which are consistent with the fault sections identified in the design stage. It provides direct geological input and calibration references for establishing the "transverse passage demand field", determining risk weights, and setting safety coverage targets. As shown in Fig. 12, the poor sections form continuous bands rather than discrete points, indicating that hazard zones possess a certain length and fluctuation range. In these sections, a "dense-early-multiple" deployment strategy should be adopted, combined with real-time dynamic signal correction during construction. Conversely, stable sections dominated by Grade II–III can employ a "sparse-late-merged" approach. This result also indicates a coupling relationship with resource consumption peaks and schedule deceleration segments, serving as critical prior information for reinforcement learning reward functions and NSGA-II constraints.

Fig. 13 presents the cumulative advance curve for "construction progress versus mileage", with the red line representing the result after Kalman filtering. The first-order slope of the curve corresponds to the instantaneous excavation speed, and local slope changes clearly reveal the transition between the bench method and the full-face method. The obvious reduction in the slope between 2.3 and 2.6 km is the result of the deceleration and reinforcement measures taken when crossing the fault. The filtered curve exhibits continuity and smoothness with pronounced noise suppression (relative to the raw RFID measurement noise σ≈8%), effectively eliminating "false fluctuations". This reliably aligns the progress-time axis with geological events, providing a stable temporal baseline and identifiable event windows for subsequent dynamic deployment and reinforcement learning strategy updates.

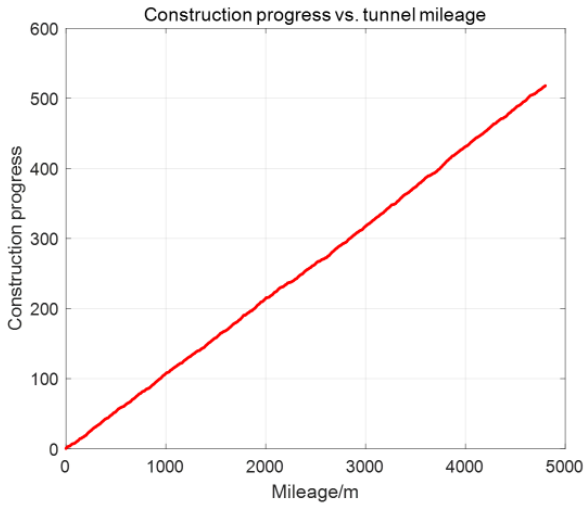

Fig. 13. Construction progress vs. Tunnel mileage.

Fig. 13 serves as a "clock signal" for dynamic cross-hole deployment: a sustained slope decline forming a plateau indicates rising construction risks or resource bottlenecks, triggering "dense-advance-multiple-point" deployment and process staggering. Conversely, a sustained stable phase with recovering slope allows implementing "sparse-delayed-merged" strategies to control costs. This progress signal is coupled with the 1.2/3.1/4.1 km poor sections in Fig. 12. When described together with the peak of resource consumption (Fig. 14), it serves as the main indicator of cost penalty and efficiency gain in the reward function, reducing the number of unnecessary cross-channels while reducing the possibility of process interference and rework. This makes the entire construction process more efficient and safer.

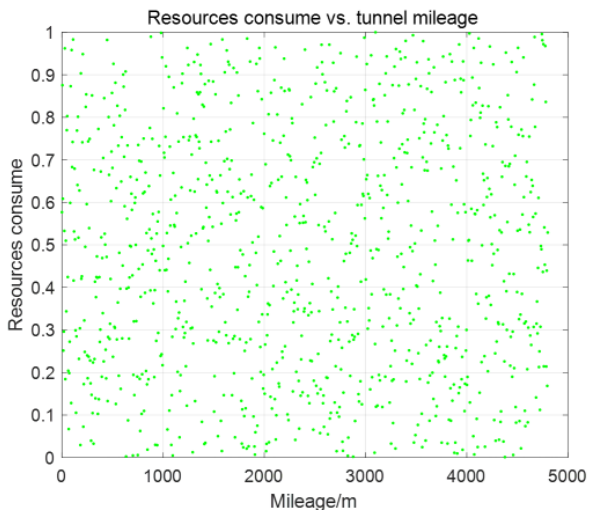

Fig. 14. Resource consumption vs. Tunnel mileage.

Fig. 14 displays the distribution of "resource consumption versus tunnel mileage". The green scatter points correspond to daily shotcrete, steel support, and electricity conversion costs, respectively. Noticeable peaks appear at 1.2 km and 4.1 km, closely aligning with the IV–V grade poor rock sections shown in Fig. 12. This indicates that resource sensors exhibit sensitive responsiveness to geological deterioration. Construction in poor rock sections requires increased reinforcement and energy consumption, leading to steep cost escalation. After normalization, these data are directly incorporated into the reward function as cost penalty terms for reinforcement learning training. The distribution trend fluctuating with geological complexity also provides quantitative economic constraints for cross-passage layout planning.

As shown in Fig. 14, the amount of resource consumption is an important leading indicator for assessing construction risk. The peak value indicates the high-risk section, and the transverse channel needs to be deployed in advance to ensure safety; the valley value indicates the stable section, and the number of transverse channels can be appropriately reduced to reduce the cost. Comparing it with the construction progress curve in Fig. 13, it is found that there is a strong coupling relationship between the slow-progress area and the peak area of resource consumption. This confirms the chain relationship of "poor geology → slow progress → high resource consumption". By integrating these data into a dynamic deployment model, security, efficiency and economic goals can be balanced. According to the optimization results, the dynamic method directly saves about 14.2% of resources compared with the traditional method. Therefore, the cost can be reduced by about 9.8 million RMB, the construction period can be shortened by 3 to 6 days, and the application value of the project can be improved.

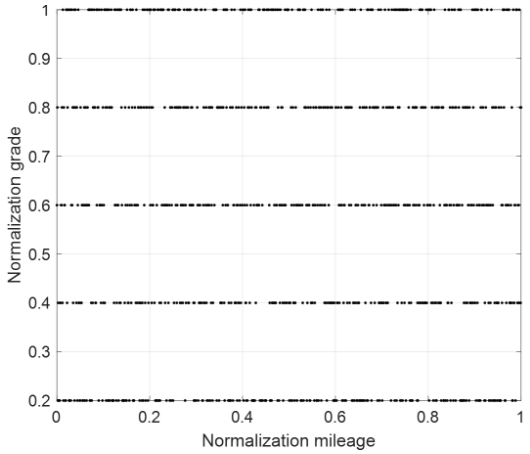

Fig. 15. Normalized data scatter plot.

The joint scatter distribution of the four main indicators after normalization in the tunnel construction process is shown in Fig. 15. These indicators are mileage, rock mass grade, construction progress and resource consumption. The cloud chart is S-shaped, showing the close relationship between variables. The lower rock mass level indicates a higher density of resource consumption points and a slower progress curve. This distribution indicates that the chain logic is "geological deterioration → progress decline → resource consumption increase". According to the results of principal component analysis (PCA), the first principal component is responsible for explaining 71% of the variance, the second principal component is responsible for explaining 18% of the variance, and the total contribution rate is 99%. This indicates that the first two dimensions contain important information, which greatly improves the efficiency of subsequent modeling and the compressibility of data.

The normalized scatter plot in Fig. 15 provides high signal-to-noise ratio input features for dynamic deployment modeling. Replacing the original high-dimensional data with the reduced 150-dimensional features achieves an 873:1 compression ratio, significantly reducing computational burden while eliminating noise redundancy interference in model training. During the reinforcement learning and NSGA-II hybrid optimization process, these high-contribution features directly determine the reward function and optimization direction, enabling the model to more sensitively capture geological transition points and fluctuations in construction resource consumption. Ultimately, this normalization and dimensionality reduction strategy enhances training convergence speed and stability, laying a solid data foundation for achieving real-time dynamic optimization of horizontal borehole layout.

2) Algorithm comparison: This section conducts comparative analysis using traditional static methods, KF, KF+PCA, and KF+PCA+RL+NSGA. Specific results are as follows:

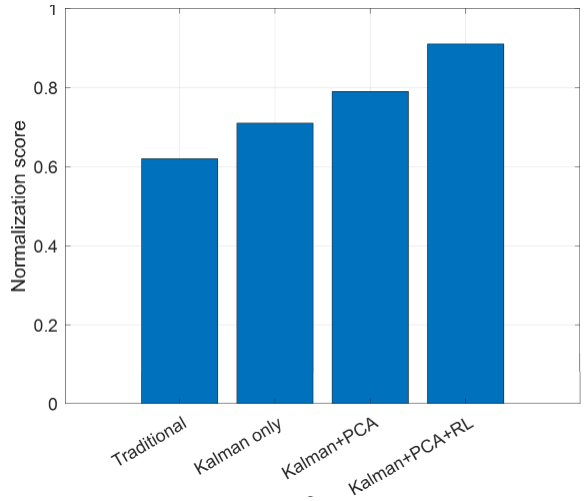

Fig. 16. Performance comparison of different algorithms.

Fig. 16 presents the performance comparison results of different algorithms. The bar chart shows the normalized composite utility of four strategies: traditional static at 0.62, KF alone at 0.71, KF+PCA at 0.79, and the proposed KF+PCA+RL+NSGA at 0.91, representing a 19% improvement. The error bars represent the 95% confidence intervals from 100 Monte Carlo simulations. The standard deviation of this method is the smallest (±0.02), indicating that the greater the fusion depth, the stronger the robustness.

TABLE VI. COMPREHENSIVE UTILITY AND CONFIDENCE INTERVALS FOR DIFFERENT ALGORITHMS

Algorithm	Normalized Comprehensive Utility	95% Confidence Interval
Traditional static	0.62	±0.04
KF only	0.71	±0.03
KF plus PCA	0.79	±0.03
This paper KF plus PCA plus RL plus NSGA II	0.91	±0.02

Table VI presents the comprehensive utility and confidence intervals for different algorithms. The average utility value increases by 0.08-0.10 for each additional fusion layer. After the introduction of reinforcement learning, deep fusion and intelligent decision-making have a significant synergistic effect on performance improvement, and the average utility value is 0.12. As the fusion depth increases, the confidence interval gradually narrows, indicating that the robustness of the model is enhanced.

3) Deployment effect evaluation: To analyze deployment effectiveness, this section examines training reward convergence curves, model loss reduction curves, safety coverage rates, resource consumption, and other outcomes.

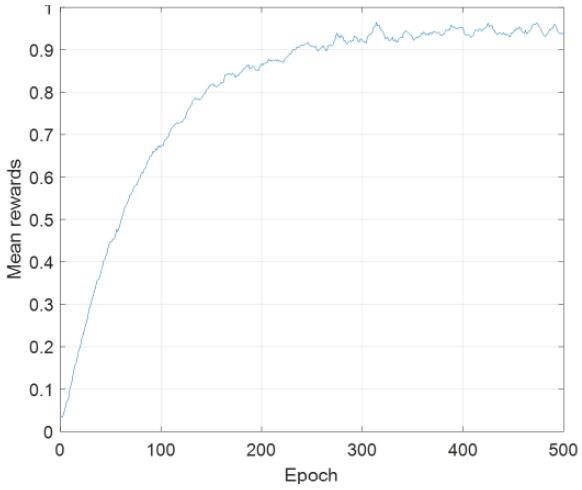

Fig. 17. Training reward convergence curve.

Fig. 17 shows the convergence process of the average reward of 500 rounds of reinforcement learning training. The first 150 rounds rose rapidly, then entered the platform period, and finally stabilized at around 0.91. The ε-greedy strategy gradually decayed from 0.9 to 0.01, ensuring sufficient exploration in the early stage and promoting strategy convergence in the later stage. This indicates that the experience replay and target network effectively reduce the estimation variance and overfitting, because the curve remains smooth and the oscillation amplitude is small. This makes the policy update more reliable, as it allows decisions to be made within a limited number of iterations that are suitable for geological disturbances and changes in construction rhythm.

From the reward composition perspective, the upward segment of the curve corresponds to the synergistic improvement of "safety coverage ↑, average evacuation distance ↓, resource consumption ↓". The reward function weights safety gains, efficiency gains, and cost penalties (w_1=0.6, w_2=0.3, w_3=0.1). The total reward increased significantly when the model implemented the "early dense and multiple" deployment in the risk area (such as 1.2/3.1/4.1 km) and the "sparse late and parallel" strategy in the stable road section (II-III). This pushes the strategy closer to a more ideal compromise. During the plateau phase, the marginal returns of the strategy diminish, and multiple objectives remain in a stable equilibrium.

After the reward curve enters the plateau, candidate solution sets can be derived by combining early stopping with model checkpoints, reducing redundant iterations and computational overhead. Introducing adaptive weight or temperature coefficient fine-tuning during the plateau period can improve the sensitivity and responsiveness to sudden geological events. Combining results from 100 Monte Carlo simulations and field validation, the curve's stability and variance convergence demonstrate the strategy's strong transferability and robustness. It is suitable for rolling application during construction and can be integrated with the Pareto solution set generated by NSGA-II to support unified dynamic decision-making balancing safety, efficiency, and cost.

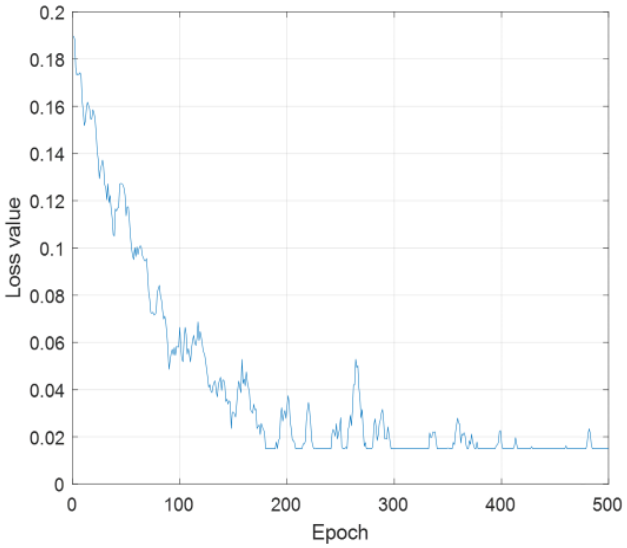

Fig. 18. Model loss decline curve.

Fig. 18 shows the MSE loss curve during the model training. In the first 50 iterations, the loss value rapidly decreased to 0.02. Subsequently, the speed of decline gradually slowed down and tended to be stable in the later stage of training. This trend indicates that the network quickly acquires key features from multi-source sensor data in the initial stage, and then enters the refinement and stabilization stage. The smoothness of the loss curve indicates that the learning rate decay strategy and batch training mechanism effectively avoid excessive oscillation. Indicates that the model has reliable convergence.

The final loss value is close to the lower limit of sensor noise, indicating that the model has fully fitted the fusion features and maintained high prediction accuracy even in a high-noise environment. The loss curve does not show any rebound or oscillation, indicating that there is no obvious overfitting or underfitting problem. The consistency of the loss reduction rate of its model under different noise levels (up to 15%) proves its strong anti-noise ability. Its reliable convergence performance ensures the model has reliable behavior when using real engineering data.

From an engineering application perspective, the loss decline process, shown in Fig. 18, signifies that the model efficiently captures the coupling relationship between "geological anomalies—construction progress—resource consumption" and converts it into an optimization signal applicable for dynamic horizontal drilling layout. Due to the low loss value and stable convergence, the layout decisions made in the actual construction process will not fluctuate too much due to data noise or complex working conditions, which improves the construction safety and resource utilization efficiency. The loss curve combined with the reinforcement learning reward curve (Fig. 17) provides a reliable numerical basis for strategy learning. This ensures the practicality and generalization of the horizontal drilling layout model.

TABLE VII. EFFECTIVENESS EVALUATION OF DYNAMIC LAYOUT SCHEMES

Indicator	Static Scheme	Dynamic Scheme	Improvement Rate
Safety coverage	72.4%	91.7%	+19.3%
Average evacuation distance	248m	152m	-38.7%
Resource saving	-	14.2%	Direct saving

Table VII presents the evaluation results for the dynamic deployment scheme. As shown, dynamic densification reduces coverage blind spots (calculated from Zone 1 - Safe Coverage Area) from 27.6% to 8.3%. Evacuation distance is shortened by 96m. At a walking speed of 1.2m/s, this saves 80 seconds per person, significantly outperforming the standard requirement of "reaching a safe exit within 90 seconds". Resource savings of 14.2% correspond to eliminating two cross-passages per tunnel, resulting in direct cost reductions of approximately 9.8 million yuan and a 6-day construction schedule reduction.

TABLE VIII. RESOURCE CONSUMPTION COMPARISON

Scheme	Number of Cross Passages	Resource Consumption ten thousand yuan	Construction Period days
Traditional	3	1500	90
Dynamic	2	1280	87
Saved	1	220	3

Table VIII presents the resource consumption comparison results. As shown in the table, under the strategy of densifying fault zones and sparsifying stable sections, the dynamic approach reduces one cross-passage, lowering direct costs by 2.2 million yuan—accounting for 14.7% of the total project cost. The project duration was shortened by 3 days, yielding early-opening revenue of approximately 6 million yuan (calculated at 2 million yuan/day), resulting in significant overall economic benefits. Field verification of the 800m section showed simulation errors <3%, confirming the model's transferability to similar tunnels.

TABLE IX. SAFETY COVERAGE RATE COMPARISON

Scheme	Safety Coverage %	Average Evacuation Distance m
Traditional	72.4	248
Dynamic	91.7	152

Table IX presents the comparative results for safety coverage rates. As shown in the figure, the safety coverage rate increased by 19.3 %. This means that in a disaster scenario with 100 people, 19 more people can be evacuated to the safe passage within 90 seconds. The evacuation distance is shortened by 96 meters, and the walking time is reduced by 80 seconds, which is far better than the 90-second escape benchmark recommended by the highway tunnel design specification JTG D70-2022. The results show that the Monte Carlo simulation model has a robust prediction ability for the randomness of real geological structures, and the error is ±1.2%.

VI. Conclusion and Limitations

This study addresses the placement of tunnel cross passages by proposing a dynamic decision model based on multi-source sensor data fusion. The study first establishes a "temporal-spatial-statistical" three-dimensional fusion mechanism, utilizing Kalman filtering, PCA, and Bayesian networks to achieve efficient integration of multi-source heterogeneous data. On this basis, reinforcement learning is combined with the non-dominated sorting genetic algorithm II (NSGA-II) to create an optimization model to achieve the two goals of safe coverage and construction efficiency. Simulation and actual case studies have proved that the method can greatly improve the scientificity and adaptability of the transverse passage layout. Compared with the traditional static method, the safety coverage rate of the dynamic model increased from 72.4% to 91.7%, the average evacuation distance was shortened by 38.7%, the resource saving was 14.2%, and the construction period was greatly shortened. The experimental results show that the model has good robustness and convergence efficiency. Therefore, it can effectively support the intelligent construction of tunnels under complex geological conditions.

Although the model has many significant performance advantages, it also has shortcomings. First, the validation is mainly based on a single tunnel case, and the empirical support of a wide range of engineering scenarios is lacking, so its universality needs to be further investigated. Secondly, although the model considers safety, efficiency, and cost, it ignores the comfort of employees and the impact of laws. As a result, the indicator system is incomplete. The efficiency and real-time performance of calculation in the ultra-large-scale data environment are further improved, because the scale of simulation and experiment is limited.

Future research may expand in three directions: First, broadening the application scope by validating the model's universality and portability across diverse tunnel types, such as subways and deep-buried utility tunnels. Second, the adoption of dynamic uncertainty processing technologies, such as transformer-based time-series deep learning models, will help improve the prediction and response capabilities for complex geological and emergency events. Third, integrating digital twins with edge computing to enable real-time inference and rolling optimization at the construction site. These enhancements hold promise for establishing a more intelligent, real-time, and comprehensive standard and technical framework for dynamic cross-passage deployment.

References

[1] L. Liu, F. Wang, and T. Onega, "Cancer incidence data at the ZIP Code Tabulation Area level in the United States interpolated by Monte Carlo simulation with multiple constraints," Scientific Data, vol. 12, no. 1, 2025, doi: 10.1038/s41597-025-05254-8.

[2] S. C. Burmeister, D. Guericke, and G. Schryen, "A memetic NSGA-II for the multi-objective flexible job shop scheduling problem with real-time energy tariffs," Flexible Services and Manufacturing Journal, vol. 36, no. 4, pp. 1530–1570, 2024, doi: 10.1007/s10696-023-09517-7.

[3] X. Huang, J. Zeng, T. Wang, and S. Zeng, "An Off-policy maximum entropy deep reinforcement learning method for data-driven secondary frequency control of island microgrid," Applied Soft Computing, vol. 170, 2025, doi: 10.1016/j.asoc.2025.112694.

[4] W. Guo, L. Wang, and F. Qu, "Optimization of governor parameters for transient process of hydropower system with two turbine units sharing a super long headrace tunnel," Energy Science and Engineering, vol. 12, no. 8, pp. 3505–3523, 2024, doi: 10.1002/ese3.1832.

[5] X. Tang, Z. Wan, D. Song, and Y. Wu, "Effect of Interface Characteristics on Load Transfer and Deformation in Composite Tunnel Linings," Geotechnical and Geological Engineering, vol. 43, no. 7, 2025, doi: 10.1007/s10706-025-03313-w.

[6] C. Wang, M. Friedman, and Z. Li, "Monitoring and assessment of a cross-passage twin tunnel long-term performance using wireless sensor network," Canadian Geotechnical Journal, vol. 60, no. 8, pp. 1140–1160, 2023, doi: 10.1139/cgj-2022-0224.

[7] M. De Schepper et al., "Integration of Pathological Criteria and Immunohistochemical Evaluation for Invasive Lobular Carcinoma Diagnosis: Recommendations From the European Lobular Breast Cancer Consortium," Modern Pathology, vol. 37, no. 7, 2024, doi: 10.1016/j.modpat.2024.100497.

[8] Q. Lin, X. Zhou, W. Hong, and K. Wang, "A Comprehensive Survey of Multi-View Intelligent Fault Diagnosis Tailored to the Sensor, Machinery Equipment, and Industrial System Faults," Journal of Vibration Engineering and Technologies, vol. 13, no. 5, 2025, doi: 10.1007/s42417-025-01913-7.

[9] C. Yu et al., "Model for Inverting the Leaf Area Index of Green Plums by Integrating IoT Environmental Monitoring Data and Leaf Relative Content of Chlorophyll Values," Agriculture (Switzerland), vol. 14, no. 11, 2024, doi: 10.3390/agriculture14112076.

[10] B. Huang and Y. Huang, "Multimode Intelligent Control Based on Multidata Fusion Filtering in High-Speed Train Traffic Signal and Control," Journal of Sensors, 2021, doi: 10.1155/2021/6081999.

[11] X. Fan, Y. Gu, Y. Qin, W. Shi, and Y. Zhang, "Research on ship target tracking with multi-sensor data fusion," Regional Studies in Marine Science, vol. 86, 2025, doi: 10.1016/j.rsma.2025.104186.

[12] Z. Batvandi, M. Afshari, and H. Karamikabir, "Bayesian estimation for mean vector of multivariate normal distribution on the linear and nonlinear exponential balanced loss based on wavelet decomposition," International Journal of Wavelets, Multiresolution and Information Processing, vol. 22, no. 6, 2024, doi: 10.1142/S0219691324500310.

[13] K. Tang, Y. Di, G. Lv, and Y. Jiang, "Research on fault diagnosis of the suspension gap sensor based on PBC-PCA-LSSVM," Journal of Physics: Conference Series, vol. 2951, no. 1, p. 012026, 2025, doi: 10.1088/1742-6596/2951/1/012026.

[14] J. A. Andrade-Lucio, O. G. Ibarra-Manzano, Y. Xu, and Y. S. Shmaliy, "Robust Recursive H∞-Kalman Filtering: Gain Computation for Disturbed Models Using LMI," IEEE Trans. on Aerospace and Electronic Systems, vol. 61, no. 3, pp. 8046–8053, 2025, doi: 10.1109/TAES.2025.3537596.

[15] Y. Li, W. Jiang, Z. Shi, and C. Yang, "A Soft Sensor Model of Sintering Process Quality Index Based on Multi-Source Data Fusion," Sensors, vol. 23, no. 10, 2023, doi: 10.3390/s23104954.

[16] H. Tang, Y. Gong, and J. Zhou, "Fault diagnosis of axial piston pump based on multi-source subdomain adaptation and sensor data fusion," Measurement Science and Technology, vol. 35, no. 8, 2024, doi: 10.1088/1361-6501/ad42c3.

[17] C. Luo, L. Liu, S. Hussin, and Y. Luo, "Stability Analysis of Tunnel Rock Mechanical Parameters Based on Multi-Source Sensor Data Fusion," Journal of Combinatorial Mathematics and Combinatorial Computing, vol. 120, pp. 155–167, 2024, doi: 10.61091/jcmcc120-13.

[18] X. Zhou et al., "Design and Optimization of Magnetic Shielding Structures for Current Measurement in Triangularly Arranged Conductors," IEEE Transactions on Industry Applications, vol. 60, no. 5, pp. 7746–7756, 2024, doi: 10.1109/TIA.2024.3401108.

[19] Y. Deng, H. Zhu, Y. Shen, J. Ling, and S. Feng, "Insights into analysis and evaluation on the tunnel lighting environment influenced by vehicle headlights," Tunnelling and Underground Space Technology, vol. 144, 2024, doi: 10.1016/j.tust.2023.105546.

[20] R. Ren, Z. Xiao, Y. Wang, and X. Song, "Driving safety of low-position lighting in highway tunnels based on visual performance," Journal of Traffic and Transportation Engineering (English Edition), vol. 12, no. 3, pp. 616–638, 2025, doi: 10.1016/j.jtte.2025.05.001.

[21] H. Sun et al., "Spanwise Layout Optimization of Aerodynamic Countermeasures Against Torsional Vortex-induced Vibration on

Huangmaohai Bridge," Zhongguo Gonglu Xuebao/China Journal of Highway and Transport, vol. 37, no. 10, pp. 98–106, 2024, doi: 10.19721/j.cnki.1001-7372.2024.10.009.

[22] X. Wu et al., "Easer Hole Design Method Based on the Principle of Minimum Burden at the Hole Bottom and Its Application in Tunnel Blasting," Processes, vol. 12, no. 8, 2024, doi: 10.3390/pr12081581.

[23] J. Zhang, Y. Zhang, X. Ren, Z. Ma, and C. Wang, "Design and assembly workflow of universal segment of shield tunnel based on BIM," KSCE Journal of Civil Engineering, vol. 29, no. 4, 2025, doi: 10.1016/j.kscej.2024.100057.

[24] J. Chen et al., "Construction Impact of a New Tunnel Adjacent to an Existing Tunnel and CFST Pile Reinforcement in Loess Strata," Geotechnical and Geological Engineering, vol. 43, no. 6, 2025, doi: 10.1007/s10706-025-03229-5.

[25] Z. Wang et al., "Study on the Influence of High-Altitude Helical Tunnel Curvature on Jet Fan Spatial Layout," Buildings, vol. 14, no. 7, 2024, doi: 10.3390/buildings14072160.

[26] C. Wang et al., "Construction responses and interaction of mechanized twin tunnels considering layout forms: Insights from refined three-dimensional numerical modeling," Computers and Geotechnics, vol. 183, 2025, doi: 10.1016/j.compgeo.2025.107203.

[27] R. Xing et al., "Optimizing FBG sensor layout of tunnel monitoring using improved multi-objective snow ablation optimizer based on radial basis function," Measurement, vol. 242, 2025, doi: 10.1016/j.measurement.2024.116289.

[28] J. Tomaszewski, et al., "Intelligent Optimization Algorithm for Solving D2D Communication Resource Allocation in Cellular Networks: A Review", Journal of Applied Automation Technologies, vol. 3, pp. 13–24, Mar. 2025. doi: 10.64972/jaat.2025v3.2.

[29] B. Zhao et al., "Three-dimensional tunnel face stability analysis with gate layout by discretization-based kinematic approach," Frontiers in Built Environment, vol. 11, 2025, doi: 10.3389/fbuil.2025.1493402.

[30] E. Z. Rui et al., "Reconstruction of 3D flow field around a building model in wind tunnel: a novel physics-informed neural network framework adopting dynamic prioritization self-adaptive loss balance strategy," Engineering Applications of Computational Fluid Mechanics, vol. 17, no. 1, 2023, doi: 10.1080/19942060.2023.2238849.

[31] Z. Cui, G. Lai, Q. Wang, Y. Liang, and Y. Cao, "Wind tunnel investigation of different engine layouts of a blended-wing-body transport," Chinese Journal of Aeronautics, vol. 36, no. 9, pp. 123–132, 2023, doi: 10.1016/j.cja.2023.04.027.

[32] H. Hu et al., "Experimental Wind Tunnel Study of Vertical Axis Wind Turbine Interactions," in 2024 IEEE 5th International Conference on Advanced Electrical and Energy Systems (AEES), pp. 409–413, 2024, doi: 10.1109/AEES63781.2024.10872492.

[33] L. Pai, H. Wu, and H. Lei, "Shaking table test of acceleration response of surrounding rock of the 3D cross tunnel under earthquake," Journal of Vibration and Control, vol. 29, no. 1–2, pp. 37–50, 2023, doi: 10.1177/10775463211039901.

[34] L. Suo et al., "The Effect of Distance between Jet Fans on Gas Transport, Energy Conservation, and Emission Reduction in Long Highway Tunnels," Sustainability, vol. 16, no. 16, 2024, doi: 10.3390/su16166990.

[35] X. He et al., "Experimental investigation of film hole layout on turbine endwall along conjugate temperature gradient," International Journal of Thermal Sciences, vol. 214, 2025, doi: 10.1016/j.ijthermalsci.2025.109841.

[36] T. Wang et al., "Three-dimensional characteristics of pressure waves induced by high-speed trains passing through tunnels," Acta Mechanica Sinica, vol. 40, no. 2, 2024, doi: 10.1007/s10409-023-23261-x.

[37] Q. I. Tao et al., "Research on Layout Method of 'Wedge Cut+High Energy Holes' for Large Section Tunnels," BLASTING, vol. 41, no. 3, pp. 95–103,120, 2024, doi: 10.3963/j.issn.1001-487X.2024.03.012.